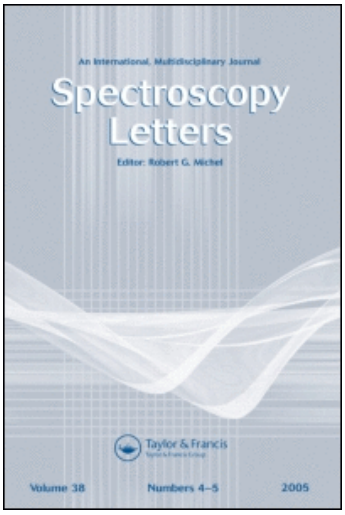

Spectroscopy Letters
Publication details, including instructions for authors and subscription information:
http://www.informaworld.com/smpp/title~content=t713597299

Accurate Determination of Rare Earth Elements in USGS, NIST SRM, and MPI-DING Glasses by Excimer LA-ICP-MS at High Spatial Resolution

Zhaochu Hu[ab]; Shan Gao[ab]; Yongsheng Liu[a]; Haihong Chen[a]; Shenghong Hu[a]
[a] State Key Laboratory of Geological Processes and Mineral Resources, Faculty of Earth Sciences, China University of Geosciences, Wuhan, People's Republic of China [b] State Key Laboratory of Continental Dynamics, Department of Geology, Northwest University, Xi'an, People's Republic of China

To cite this Article Hu, Zhaochu , Gao, Shan , Liu, Yongsheng , Chen, Haihong and Hu, Shenghong(2008) 'Accurate Determination of Rare Earth Elements in USGS, NIST SRM, and MPI-DING Glasses by Excimer LA-ICP-MS at High Spatial Resolution', Spectroscopy Letters, 41: 5, 228 — 236
To link to this Article: DOI: 10.1080/00387010802171951
URL: http://dx.doi.org/10.1080/00387010802171951

Spectroscopy Letters, 41:228–236, 2008

ISSN: 0038-7010 print/1532-2289 online
DOI: 10.1080/00387010802171951

Taylor & Francis
Taylor & Francis Group

Accurate Determination of Rare Earth Elements in USGS, NIST SRM, and MPI-DING Glasses by Excimer LA-ICP-MS at High Spatial Resolution

Zhaochu Hu[1,2], Shan Gao[1,2], Yongsheng Liu[1], Haihong Chen[1], and Shenghong Hu[1]

[1]State Key Laboratory of Geological Processes and Mineral Resources, Faculty of Earth Sciences, China University of Geosciences, Wuhan, People's Republic of China
[2]State Key Laboratory of Continental Dynamics, Department of Geology, Northwest University, Xi'an, People's Republic of China

ABSTRACT The effect of central gas flow rate (carrier gas and makeup gas) on signal intensities, ThO/Th, Th/U, memory effect, and interface pressures were investigated in this work. Detailed examination of the changing trend of fractionation index with different crater diameters from 8 μm to 60 μm reveals that rare earth elements (REEs) can also be classified into three groups: (1) La, Pr, Nd, and Sm (light REEs), (2) Ce, and (3) Eu, Gd, Tb, Dy, Ho, Er, Tm, Yb, and Lu (heavy REEs). In this work, REEs in MPI-DING glasses, USGS basaltic reference glasses, and the synthetic NIST glasses were determined at a high spatial resolution of 24 μm. The limits of detection for REEs at a spot size of 24 μm are within the range 0.003 to 0.030 μg g^{-1}. Most of the determined values were found to be in excellent agreement with the reference values, with the relative error (RE) less than 10%. Our analytical precision, as given by the 1-s relative standard deviation (% RSD), is typically less than 15% for elements having concentration higher than 0.1 μg g^{-1}, and there is a significant negative correlations between concentration and RSD on a logarithmic scale for these glasses, with logarithmic correlation coefficients being −0.84. This expected trend of decreasing RSD with increasing concentration for these glasses indicates that the analytical precision follows counting statistics and thus that most of the data variation is analytical in origin and not due to chemical heterogeneities. Ce in GOR132-G is a notable exception, which has especially high RSD, and thus is possibly not homogeneously distributed.

KEYWORDS LA-ICP-MS, MPI-DING glasses, NIST SRM 610–614, trace elements, USGS glasses

Received 31 May 2007; accepted 9 January 2008.

Address correspondence to Zhaochu Hu, State Key Laboratory of Geological Processes and Mineral Resources, Faculty of Earth Sciences, China University of Geosciences, Wuhan, 430074, People's Republic of China. E-mail: zchu@vip.sina.com

INTRODUCTION

Laser ablation–inductively coupled plasma-mass spectrometry (LA-ICP-MS) has become one of the powerful techniques for *in situ* analysis of chemical and isotopic compositions for a wide variety of materials.[1–3]

Early limitations of LA-ICP-MS, such as poor absorption of the laser energy by transparent samples, nonhomogeneous energy distribution on the sample surface, limited spatial resolution, and fluency-related ablation characteristics, have been well studied and considerable progress has been made, particularly with the developments of powerful UV-laser ablation systems and ICP-MS instruments.[1–6] However, time-dependent signal ratio variation, so-called elemental fractionation, has remained as one of the major limitations of the technique. Elemental fractionation represents the sum of all nonstoichiometric effects occurring during the ablation process, transport to and ionization in the ICP source. This is especially problematic for quantitative analysis, when matrix-matched calibration reference materials are not available. Previous work indicates that changing the wavelength from IR towards UV and deep UV has successfully reduced this effect.[1–6]

Rare earth elements (REEs) are widely used as geochemical indicators in petrogenetic studies of magmatic rocks and as tracers of geochemical processes in crust–mantle system. The accurate analysis of REEs is considered prerequisite in these investigations. LA-ICP-MS has been successfully used for the determination of REEs, which are usually difficult for solution-nebulization ICP-MS due to the presence of hard-to-digest minerals such as garnet and zircon. In this study, the interelement fractionation behaviors of REEs were studied by adopting single-hole ablation combined with using different crater diameters from 8 μm to 60 μm, and the optimum central gas flow rate for excimer laser-induced aerosol introduced into an ICP-MS was also investigated. REEs in the MPI-DING glasses, USGS basaltic reference glasses, and the synthetic NIST glasses were determined at a high spatial resolution of 24 μm, and concentrations are compared with reference values from the literature. The individual concentrations and deviations from the previously reported values are also discussed.

MATERIALS AND METHODS

Instrumentation

Experiments were carried out on an Agilent 7500a ICP-MS instrument (Yokogawa, Japan) in combination with an excimer 193-nm laser ablation system (GeoLas 2005). All LA-ICP-MS measurements were carried out using time-resolved analysis that operated in a fast, peak-jumping mode. Each spot analysis consisted of approximately 30-s background acquisition followed by 40-s data acquisition from the sample. Details of the instrumental operating conditions and measurement parameters are reported in Table 1. Because of small sample quantities that are removed during laser ablation at high spatial resolution, a high sensitivity is essential for trace and ultratrace analysis in practical samples. Therefore, the shielded torch was activated in this study. Helium was used as carrier gas within the ablation cell and was merged with argon (makeup gas) behind the ablation cell. As shown by previous studies,[7,8] for the 193-nm laser a consistent two to three fold signal enhancement was achieved in helium above that in argon gas.

TABLE 1 Summary of the operating conditions used for LA-ICP-MS measurements

GeoLas 2005 Laser ablation system	
Wavelength	193 nm, excimer laser
Repetition rate	8 Hz
Pulse length	15 ns
Energy density	20 J cm^{-2}
Spot sizes	8, 16, 24, 32, 44, and 60 μm
Ablation cell gas	Helium
Makeup gas	Argon
Agilent 7500a ICP-MS	
RF power	1350 W
Plasma gas flow rate	14.0 L min^{-1}
Auxiliary gas flow rate	1.0 L min^{-1}
Sampling depth[a]	5.4 mm
Shielded torch	Activated
Ion optic settings	Typical
Isotopes measured	^{42}Ca, ^{139}La, ^{140}Ce, ^{141}Pr, ^{143}Nd, ^{147}Sm, ^{151}Eu, ^{155}Gd, ^{159}Tb, ^{163}Dy, ^{165}Ho, ^{166}Er, ^{169}Tm, ^{173}Yb, ^{175}Lu, ^{232}Th, ^{238}U
Dwell time per isotope	10 ms
Detector mode	Dual

[a]Software setting. True value is approx. + 5 mm.

Samples

Polished NIST SRM 610 was used to study the elemental fractionation because it is one of the well

characterized and most widely used reference materials in LA-ICP-MS. To investigate the accuracy and precision of 193-nm ArF excimer lasers for high spatial resolution analysis, the MPI-DING glasses (ATHO-G [rhyolite], GOR128-G [komatiite], GOR132-G [komatiite], KL2-G [basalt], ML3B-G [basalt], StHs6/80-G [andesite] and T1-G [quartz-diorite]), USGS basaltic reference glasses (BCR-2G, BHVO-2G, and BIR-1G), and the synthetic NIST glasses (610, 612, and 614) were used, for which reliable reference data exist.[9–12]

Data Reduction and Quantification

Data reduction was made using GLITTER 4.4 software (Macquarie University). Calibration was performed using NIST SRM 610 as an external calibration sample in conjunction with internal standardization using Ca. Concentration values of NIST SRM 610 used for external calibration in GLITTER 4.4 software were taken from Pearce et al.[9]

RESULTS AND DISCUSSION

Optimization of the Central Gas Flow Rate

As laser ablation becomes more ubiquitous for direct solid sampling with ICP-MS, the need to mitigate fractionation is critical. ICP-induced elemental fractionation can be reduced when the operating parameters are optimized to generate a sufficient gas temperature in the central channel of the ICP.[6,13,14] Generally, a lower nebulizer gas flow rate and higher RF power are facilitated to reduce ICP-induced elemental fractionation.[6,13] Kuhn et al.[14] compared ionization efficiencies using different plasma forward powers. Their results showed that the energy transfer at 1000 W is less suitable to vaporize and ionize particles than at 1300 W, and 1600 W is somewhere in between the two other settings. The central gas flow rate is another key plasma operating parameter affecting analyte ion signals in LA-ICP-MS.[6,13] To describe the processes in the plasma in detail, U and Th were often used as indicators because of their very similar ionization potentials, mass number, and their almost identical concentrations within the NIST SRM 610.[6] Figure 1 shows the changing of Th/U ratio, normalized La and Lu signal, and ThO/Th ratio with makeup gas flow rate

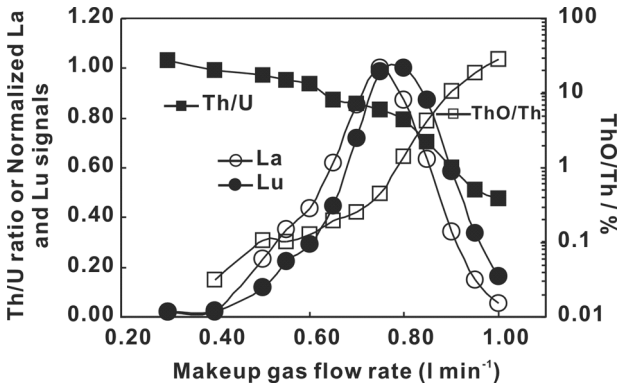

FIGURE 1 **Dependence of U/Th ratio, normalized La and Lu signals, and ThO/Th ratio on makeup gas flow rate during single-hole laser ablation sampling at a crater diameter of 24 μm. Signals of La and Lu are normalized to their highest values.**

during a single-hole ablation (24 μm) at normal RF power of 1350 W. It can be seen that the Th/U ratio is significantly decreased with increasing makeup gas flow rate. The selection of the optimal makeup gas flow rate to eliminate ICP-induced fractionation ($Th/U \approx 1$) in this example is accompanied by as much as 70% reduction in La and Lu sensitivities. Therefore, the reduction of ICP-induced elemental fractionation by selecting operating parameters was compromised. A makeup gas flow rate of 0.75 L min^{-1} was selected in practical sample analysis in terms of the La and Lu sensitivities and ThO/Th ratio (0.45%). Similar signal variations can also be obtained by changing the carrier gas flow rate at a given makeup gas flow rate. In this study, the carrier gas flow rate was fixed at 0.70 L min^{-1}. As shown in Fig. 2, it will take 40 s for the signal reduction by two orders of magnitude at the carrier gas flow rate of 0.40 L min^{-1}, whereas it only needs 15 s at

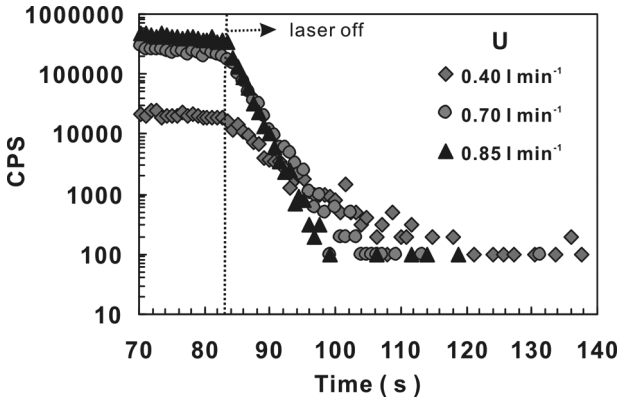

FIGURE 2 **Effect of carrier gas flow rate (He) on the memory effect.**

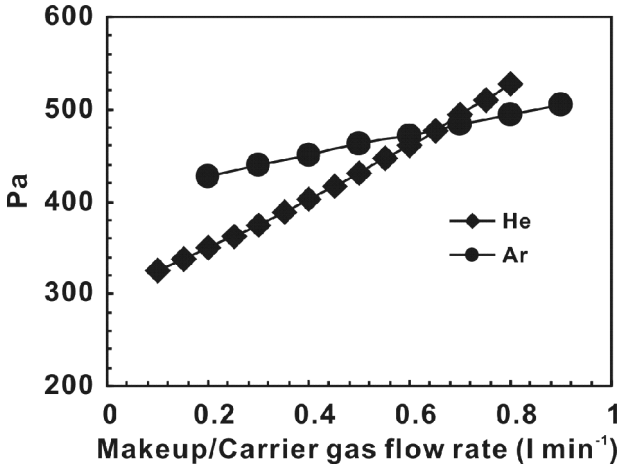

FIGURE 3 Effect of carrier gas flow rate (He) and makeup gas flow rate (Ar) on the vacuum pressure of the interface.

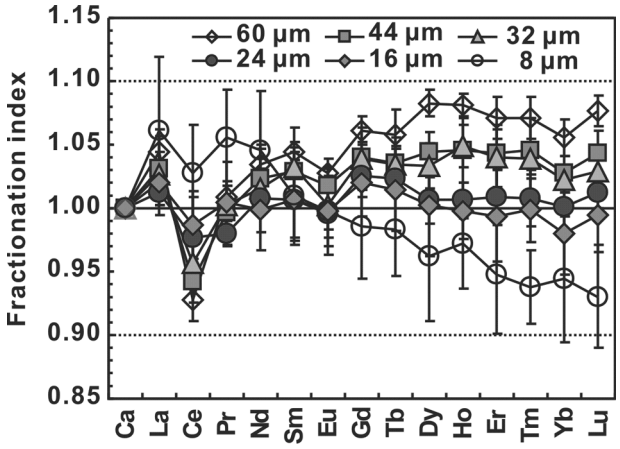

FIGURE 4 Variations of fractionation indices (FIs) of REEs with crater diameters. The FIs are defined as the ratio of the calcium normalized signal in the second 20 s of the ablation divided by the calcium normalized signal in the first 20 s of the ablation, as described by Fryer et al.[15] Data were generated on NIST SRM 610.

0.70 L min^{-1}. Although the increased carrier gas flow rate facilitates the reduction of memory effect, the vacuum pressure of the interface is getting worse. With the increase of gas flow rate by 0.1 L min^{-1}, the interface vacuum pressure is increased to a higher value by about 30 Pa for He (carrier gas), whereas the corresponding increase by Ar (makeup gas) is only about 11 Pa (Fig. 3). By adopting a new sampling cone, the maximum carrier gas flow rate can approach to 0.85 L min^{-1} without extinguishing the plasma (makeup gas flow rate was fixed at 0.75 L min^{-1}). In our laboratory, we have to change the sampling cone every half-years for LA-ICP-MS analysis due to the gradually enlarged cone orifice, which, subsequently, would seriously jeopardize the interface vacuum pressure. The significant improved interface pressure with increasing carrier gas flow rate (He) should be attributed to the high diffusion coefficient of He, which makes it relatively difficult to be removed by the mechanical pump.

Interelement Fractionation

Despite many successful approaches and even quantification without standards, elemental fractionation still remains the main focus in studies of LA-ICP-MS.[3] For accurate calibration, especially where matrix and ablation conditions are not perfectly matched between reference material and sample, use of an internal standard with similar ablation behaviors and excitation characteristics within the plasma to the elements of interest is essential.[15] Several studies have been carried out to correlate physical properties of elements to the degree of laser ablation–induced elemental fractionation (e.g., boiling points, melting points, ionization potential, condensation temperature, ionic radii, field strength.[16–20] However, it becomes clear from

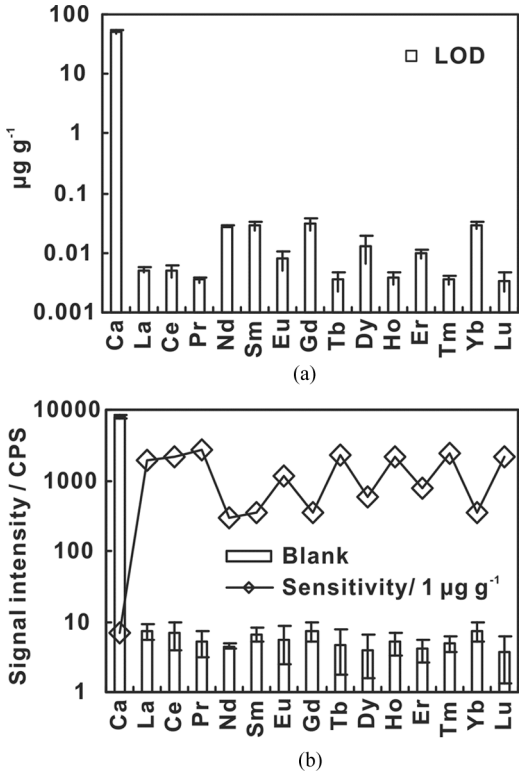

FIGURE 5 (a) Limits of detection (LODs) and (b) background intensities and analyte sensitivities for a 24-µm single-hole ablation.

TABLE 2 Analytical results for 12 silicate reference samples using LA-ICP-MS at a crater diameter of 24 μm, calibrated with NIST SRM 610 reference material and Ca as internal standard

	ATHO-G (N = 24)				GOR128-G (N = 24)				GOR132-G (N = 24)			
μg g^{-1}	This study	U	Jochum et al.[12]	U	This study	U	Jochum et al.[12]	U	This study	U	Jochum et al.[12]	U
La	58.4	1.1	55.6	1.5	0.12	0.01	0.121	0.004	0.088	0.007	0.0842	0.0029
Ce	122	2	121	4	0.43	0.02	0.45	0.016	0.51	0.08	0.393	0.018
Pr	14.2	0.3	14.6	0.4	0.092	0.006	0.1	0.004	0.088	0.005	0.089	0.004
Nd	61.2	1.2	60.9	2	0.79	0.05	0.784	0.047	0.72	0.05	0.689	0.017
Sm	14.4	0.4	14.2	0.4	0.51	0.04	0.525	0.02	0.53	0.04	0.508	0.015
Eu	2.83	0.06	2.76	0.1	0.28	0.02	0.264	0.008	0.26	0.02	0.255	0.007
Gd	15.0	0.4	15.3	0.7	1.12	0.08	1.17	0.04	1.09	0.07	1.19	0.04
Tb	2.52	0.05	2.51	0.08	0.25	0.01	0.248	0.012	0.26	0.02	0.269	0.011
Dy	16.2	0.3	16.2	0.7	1.93	0.06	1.98	0.07	2.07	0.07	2.15	0.06
Ho	3.47	0.07	3.43	0.11	0.45	0.02	0.443	0.019	0.49	0.02	0.507	0.019
Er	9.81	0.21	10.3	0.5	1.31	0.04	1.4	0.06	1.48	0.05	1.56	0.05
Tm	1.46	0.04	1.52	0.07	0.20	0.01	0.204	0.009	0.22	0.01	0.234	0.009
Yb	10.4	0.2	10.5	0.4	1.39	0.06	1.41	0.06	1.56	0.07	1.61	0.04
Lu	1.51	0.04	1.54	0.05	0.20	0.01	0.206	0.009	0.22	0.01	0.237	0.009

	KL2-G (N = 24)				ML3B-G (N = 24)				StHs6/80-G (N = 24)			
μg g^{-1}	This study	U	Jochum et al.[12]	U	This study	U	Jochum et al.[12]	U	This study	U	Jochum et al.[12]	U
La	13.4	0.2	13.1	0.2	9.31	0.17	8.99	0.13	12.6	0.2	12	0.3
Ce	32.2	0.5	32.4	0.7	23.0	0.5	23.1	0.3	26.2	0.4	26.1	0.7
Pr	4.34	0.08	4.6	0.1	3.21	0.05	3.43	0.06	3.02	0.06	3.2	0.06
Nd	21.1	0.5	21.6	0.4	16.7	0.4	16.7	0.2	13.1	0.3	13	0.3
Sm	5.49	0.14	5.54	0.09	4.76	0.13	4.75	0.07	2.84	0.11	2.78	0.05
Eu	1.97	0.05	1.92	0.04	1.73	0.04	1.67	0.02	0.99	0.04	0.953	0.022
Gd	5.54	0.17	5.92	0.2	5.01	0.18	5.26	0.23	2.56	0.14	2.59	0.09
Tb	0.84	0.03	0.89	0.031	0.80	0.02	0.797	0.021	0.37	0.02	0.371	0.011
Dy	4.93	0.13	5.22	0.12	4.73	0.12	4.84	0.07	2.15	0.08	2.22	0.06
Ho	0.94	0.02	0.961	0.022	0.89	0.03	0.906	0.018	0.42	0.02	0.42	0.011
Er	2.33	0.07	2.54	0.07	2.32	0.07	2.44	0.05	1.12	0.04	1.18	0.04
Tm	0.31	0.01	0.331	0.009	0.30	0.02	0.324	0.007	0.16	0.01	0.172	0.007
Yb	2.00	0.07	2.1	0.05	1.99	0.09	2.06	0.04	1.13	0.05	1.13	0.03
Lu	0.27	0.01	0.285	0.009	0.27	0.01	0.286	0.006	0.16	0.01	0.168	0.006

	T1G (N = 24)				BCR-2G (N = 42)				BHVO-2G (N = 30)			
μg g^{-1}	This study	U	Jochum et al.[12]	U	This study	U	Gao et al.[10]	U	This study	U	Gao et al.[10]	U
La	75.2	1.0	70.4	2.4	25.1	0.4	25	1	15.9	0.3	15.6	0.6
Ce	128	2	127	4	51.3	0.6	52	2	37.7	0.5	37	1
Pr	12.1	0.2	12.4	0.4	6.20	0.08	6.3	0.4	5.03	0.07	5	0.3
Nd	41.9	0.7	41.4	1.2	27.4	0.5	27	1	24.4	0.4	24	1
Sm	6.68	0.15	6.57	0.14	6.32	0.15	6.3	0.5	5.94	0.15	5.8	0.5
Eu	1.25	0.04	1.21	0.04	1.95	0.03	1.91	0.09	2.11	0.04	2	0.1
Gd	5.18	0.18	5.31	0.29	6.29	0.19	6.5	0.6	5.86	0.16	5.9	0.4
Tb	0.73	0.03	0.773	0.029	0.97	0.03	0.95	0.07	0.87	0.03	0.86	0.06
Dy	4.34	0.13	4.5	0.12	5.85	0.14	6	0.4	5.06	0.10	4.9	0.4
Ho	0.88	0.02	0.86	0.031	1.21	0.03	1.2	0.07	0.95	0.03	0.91	0.06
Er	2.45	0.06	2.49	0.08	3.24	0.08	3.3	0.2	2.33	0.06	2.3	0.2

(*Continued*)

TABLE 2 Continued

	T1G (N = 24)				BCR-2G (N = 42)				BHVO-2G (N = 30)			
$\mu g\,g^{-1}$	This study	U	Jochum et al.[12]	U	This study	U	Gao et al.[10]	U	This study	U	Gao et al.[10]	U
Tm	0.34	0.01	0.354	0.015	0.46	0.01	0.46	0.04	0.31	0.01	0.30	0.05
Yb	2.42	0.10	2.38	0.08	3.29	0.08	3.2	0.3	1.97	0.07	2.0	0.2
Lu	0.34	0.02	0.354	0.012	0.46	0.02	0.47	0.04	0.26	0.02	0.26	0.04
	BIR-1G (N = 26)				NIST SRM 612 (N = 39)				NIST SRM 614(N = 34)			
$\mu g\,g^{-1}$	This study	U	Gao et al.[10]	U	This study	U	Gao et al.[10]	U	This study	U	Gao et al.[10]	U
La	0.64	0.02	0.60	0.04	37.7	0.5	37	1	0.74	0.02	0.72	0.03
Ce	1.92	0.05	1.90	0.08	38.2	0.4	38	2	0.79	0.02	0.79	0.03
Pr	0.35	0.02	0.36	0.02	36.3	0.4	37	1	0.73	0.02	0.75	0.03
Nd	2.31	0.08	2.3	0.2	35.7	0.5	35	1	0.78	0.04	0.74	0.06
Sm	1.05	0.05	1.1	0.1	38.1	0.5	37	1	0.77	0.04	0.77	0.08
Eu	0.52	0.03	0.51	0.04	37.1	0.5	35	1	0.80	0.03	0.75	0.05
Gd	1.69	0.08	1.6	0.1	35.9	0.5	36	1	0.73	0.04	0.75	0.06
Tb	0.34	0.02	0.32	0.03	37.7	0.5	36	1	0.76	0.02	0.74	0.03
Dy	2.37	0.09	2.3	0.2	35.3	0.5	36	1	0.72	0.02	0.74	0.06
Ho	0.54	0.03	0.51	0.05	38.5	0.4	38	1	0.75	0.02	0.76	0.04
Er	1.57	0.05	1.5	0.1	36.5	0.6	37	1	0.72	0.03	0.73	0.05
Tm	0.23	0.01	0.22	0.02	36.2	0.5	37	1	0.70	0.02	0.72	0.06
Yb	1.55	0.11	1.5	0.1	39.9	0.5	40	1	0.77	0.03	0.81	0.09
Lu	0.24	0.01	0.23	0.02	36.6	0.5	37	1	0.73	0.02}	0.72	0.05

N, number of determinations; U, uncertainty at 95% confidence level (calculated in ISOPLOT 3.0[24]. Using analytical uncertainties as errors for individual data points. Concentrations are reported in $\mu g\,g^{-1}$.

evaluating various physical properties of individual elements that no single parameter alone controls fractionation.[21,22] Rather, the elements appear to be correlated most strongly according to Goldschmidt's geochemical classifications of elements (lithophile, siderophile, and chalcophile groupings)[15,22] that result from a combination of elemental properties that distribute elements within a three-phase system consisting of a silicate, a metallic Fe, and a sulfide liquid. Figure 4 shows the effect of changing crater diameters from 60 μm to 8 μm on the calculated elemental fractionation index (FI) under our given instrument conditions. The FIs for REEs were calculated, based on Ca as internal standard. To simulate real application conditions, the FIs were calculated by dividing the 40 s transient signals into two equal time intervals. The ratios to calcium of the second 20-s interval were divided by the corresponding ratio of the first time interval, as described by Fryer et al.[15] The FIs are, therefore, a measure of the fractionation of each element relative to Ca, a value of 1 indicating no relative fractionation. For lithophile elements Ca and REEs, it is expected that they will show generally similar fractionation behaviors. As shown in Fig. 4, the obtained FIs are all within the range 0.9–1.1. However, detailed examination of the changing trend of FIs with different crater diameters reveals that REEs can also be classified into three groups: (1) La, Pr, Nd, and Sm (light REEs), (2) Ce, and (3) Eu, Gd, Tb, Dy, Ho, Er, Tm, Yb, and Lu (heavy REEs) (Fig. 4). It can be seen that decreasing crater diameter leads to a gradual reduction in calculated FIs of REEs except for Ce. This is followed by a gradual increase in FIs of light REEs. In contrast with heavy REEs, the changing range for light REEs with crater diameters is considerably smaller. Unlike other REEs, the FI of Ce increases with decreasing crater diameters. It is well-known in geochemistry that Ce displays anomalous behavior by forming both trivalent and tetravalent ions in different conditions. (Note that the other REE predominaetly exist in the trivalent form.) The results presented here suggest that ionic charge may also have an effect on elemental fractionation. Further work on the species formed

during ablation and plasma-related processes are needed to identify the elemental fractionation mechanisms in LA-ICP-MS.

Detection of Limit

Excimer LA-ICP-MS has become an especially important tool for trace element analysis of geological and environmental samples at high spatial resolution, owing to the more efficient interaction of ultraviolet laser beam with solid samples and the increased sensitivity of ICP-MS. Depending on the desired spatial resolution, which determines the maximum amount of sample that can be analyzed, excimer LA-ICP-MS can achieve ng g^{-1} LOD (limit of detection) for spot sizes above 60 μm. Our obtained LODs for REEs at a spot size of 24 μm are given in Fig. 5a. The LOD was calculated according to the protocol of Longerich et al.[23] It can be seen from Fig. 5a that LODs range from 0.003 to 0.030 μg g^{-1} for REEs, whereas it is 50 μg g^{-1} for Ca. As illustrated in Fig. 5b, the high LODs are mainly a combination of high background intensities and relatively low isotope sensitivities.

Analysis of Glasses Sample at High Spatial Resolution

The greatest strength of the LA-ICP-MS technique is its application to microsampling in which extremely small pits are obtained. In this study, a spot size of 24 μm was used to test the capabilities of 193-nm excimer laser for LA-ICP-MS analysis at high spatial resolution. As already shown in Fig. 4, the calculated FIs are within the range 0.97–1.03 at the spot size of 24 μm. To demonstrate the analytical accuracy, NIST SRM 610 was used as external calibration reference and Ca as the internal standard to quantify trace element concentrations in glasses. The reference values of NIST SRM 610 are taken from Pearce et al.[9] Concentrations of REEs determined in ATHO-G, GOR128-G, GOR132-G, KL2-G, ML3B-G, StHs6/80-G, T1-G, BCR-2, BHVO-2, BIR-1, NIST SRM 612, and NIST SRM 614 are listed in Table 2. For comparison, reference values of these glasses are also presented in Table 2, which are taken from Jochum et al.[12] and Gao et al.[10] Analytical precision, as given by the 1-s relative standard deviation (% RSD), is typically less than 15% for elements having concentration higher than 0.1 μg g^{-1} (Table 2

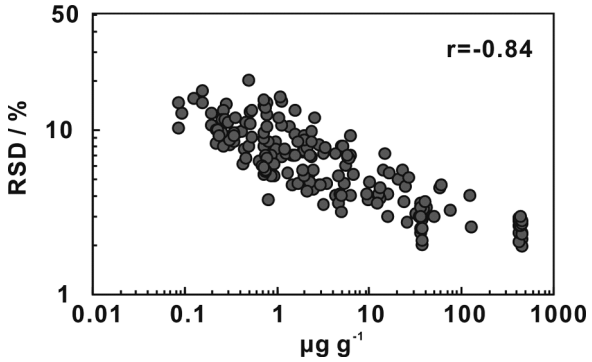

FIGURE 6 Correlation between relative standard deviation (RSD) and concentration for REEs plotted on a logarithmic scale.

and Fig. 6), and there is a significant negative correlation between concentration and RSD on a logarithmic scale for these glasses, with logarithmic correlation coefficients being −0.84 (Fig. 6). This expected trend of decreasing RSD with increasing concentration for these glasses indicates that the analytical precision follows counting statistics and thus that most of the data variation is analytical in origin and not due to chemical heterogeneities. The

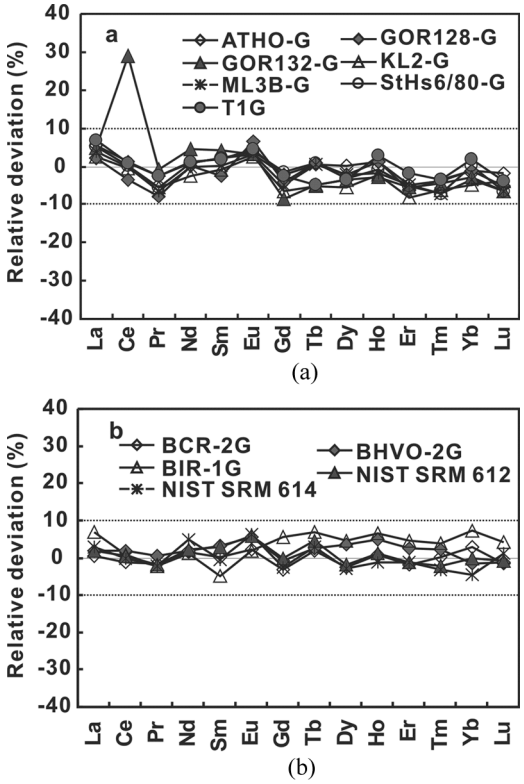

FIGURE 7 (a) Relative deviation of average concentrations in MPI-DING glasses obtained in this study from reference values of Jochum et al.[12] (b) Relative deviation of average concentrations in BHVO-2G, BCR-2G, BIR-1G, NIST SRM 612, and NIST SRM 614 obtained in this study from reference values of Gao et al.[10]

comparison of the LA-ICP-MS data with literature values[10,12] shows satisfactory agreement, with most of the determined and reference values in these glasses agreeing within 10% relative (Fig. 7). As already shown by Jochum et al.[25] who also used a 193-nm laser, different fractionation indices are observed for different matrices (on the order 1–5%). This may be one reason for the small difference of the MPI-DING glass data of this work with the reference values of Jochum et al.[12] Ce in GOR132-G is a notable exception (Fig. 7a). Our determined concentration ($0.51 \pm 0.08\,\mu g\,g^{-1}$) is higher than the reference value ($0.393 \pm 0.018\,\mu g\,g^{-1}$) by about 30%, and has especially high RSD (15%). As shown in Fig. 8a, the chondrite normalized REE pattern of GOR132-G using reference values is smoother than that using our determined values. Because our data were acquired over a period of 6 months, it is possible that the different instrument conditions may have an effect on this determined value. To eliminate this possible effect and improve the analytical precision, we performed another 60 analyses continuously on this glass sample at a larger spot size of 44 μm under the same given instrument conditions. As shown in Fig. 8b, the determined Ce values ($0.46 \pm 0.13\,\mu g\,g^{-1}$) are also highly dispersed. We thus proposed that Ce is not homogeneously distributed in this glass fragment of GOR132-G. Further investigation is required to clarify the reason. The description about the heterogeneity of this komatiite glass for other elements can be found in Jochum et al.[12,26]

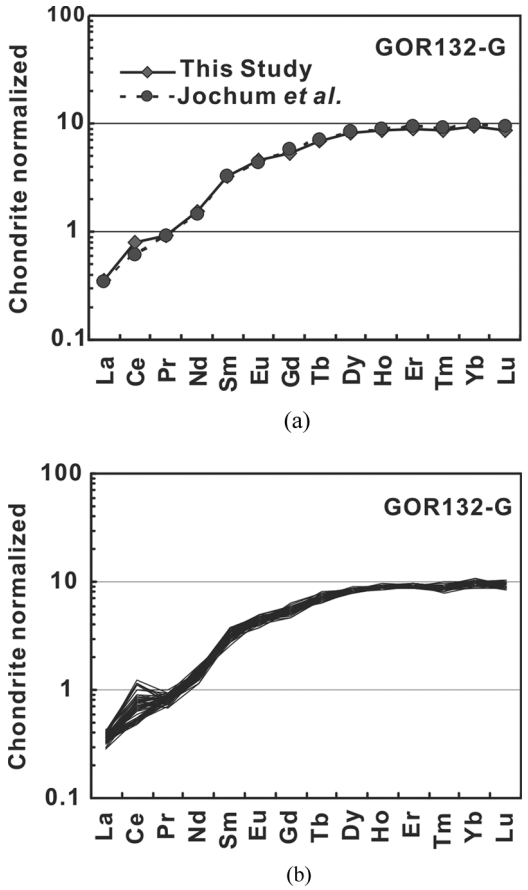

FIGURE 8 **(a) Chondrite normalized REE patterns for the determined and reference values of GOR132-G. (b) Chondrite normalized REE patterns of GOR132-G for 60 single analyses conducted in the same run at a crater diameter of 44 μm.**

CONCLUSIONS

The excellent agreement between the determined and reference values in MPI-DING glasses, USGS basaltic reference glasses, and the synthetic NIST glasses by LA-ICP-MS demonstrates the capabilities of this technique in quantitative trace element analysis at high spatial resolution of 24 μm. Analytical precision, as given by the relative standard deviation, is typically less than 15% for elements having concentration higher than $0.1\,\mu g\,g^{-1}$, and there is a significant negative correlation between concentration and RSD on a logarithmic scale for these glasses, with logarithmic correlation coefficients being -0.84. It is thus concluded that most of the data variation is analytical in origin and not due to chemical heterogeneities on a scale of 24 μm. Our LA-ICP-MS analysis result suggests that Ce is not homogeneously distributed in our glass fragment of GOR132-G.

ACKNOWLEDGMENTS

We thank Klaus Peter Jochum for providing MPI-DING reference glasses. This research is supported by the National Nature Science Foundation of China (grants 40521001, 20575061, 40673019, 90714010), the Grant Project of the Chinese Ministry of Education (B07039, IRT0441, and 306021) and China Postdoctoral Science Foundation.

REFERENCES

1. Durrant, S. F. Laser ablation inductively coupled plasma mass spectrometry: Achievements, problems, prospects. J. Anal. At. Spectrom. **1999**, *14*, 1385–1403.
2. Russo, R. E.; Mao, X. L.; Liu, H. C.; Gonzalez, J.; Mao, S. S. Laser ablation in analytical chemistry—a review. Talanta **2002**, *57*, 425–451.

3. Günther, D.; Hattendorf, B. Solid sample analysis using laser ablation inductively coupled plasma mass spectrometry. TRAC Trend. Anal. Chem. **2005**, *24*, 255–265.
4. Jeffries, T. E.; Perkins, W. T.; Pearce, N. J. G. Comparisons of infrared and ultraviolet laser probe microanalysis inductively coupled plasma mass spectrometry in mineral analysis. Analyst **1995**, *120*, 1365–1371.
5. Günther, D.; Frischknecht, R.; Heinrich, C. A.; Kahlert, H. J. Capabilities of an argon fluoride 193 nm excimer laser for laser ablation inductively coupled plasma mass spectometry microanalysis of geological materials. J. Anal. At. Spectrom. **1997**, *12*, 939–944.
6. Hattendorf, B.; Latkoczy, C.; Günther, D. Laser ablation–ICP-MS. Anal. Chem. **2003**, 341A–347A.
7. Eggins, S. M.; Kinsley, L. P. J.; Shelley, J. M. G. Deposition and element fractionation processes during atmospheric pressure laser sampling for analysis by ICP-MS. Appl. Surf. Sci. **1998**, *129*, 278–286.
8. Günther, D.; Heinrich, C. A. Comparison of the ablation behaviour of 266 nm Nd:YAG and 193 nm ArF excimer lasers for LA-ICP-MS analysis. J. Anal. At. Spectrom. **1999**, *14*, 1369–1374.
9. Pearce, N. J. G.; Perkins, W. T.; Westgate, J. A.; Gorton, M. P.; Jackson, S. E.; Neal, C. R.; Chenery, S. P. A compilation of new and published major and trace element data for NIST SRM 610 and NIST SRM 612 glass reference materials. Geostand. Newsl. **1997**, *21*, 115–141.
10. Gao, S.; Liu, X. M.; Yuan, H. L.; Hattendorf, B.; Günther, D.; Chen, L.; Hu, S. H. Determination of forty two major and trace elements in USGS and NIST SRM glasses by laser ablation-inductively coupled plasma-mass spectrometry. Geostand. Newsl. **2002**, *26*, 181–195.
11. Jochum, K. P.; Nohl, U.; Herwig, K.; Lammel, E.; Stoll, B.; Hofmann, A. W. GeoReM: A new geochemical database for reference materials and isotopic standards. Geostand. Geoanal. Res. **2005**, *29*, 333–338.
12. Jochum, K. P.; Stoll, B.; Herwig, K.; Willbold, M.; Hofmann, A. W. Forty eight others, MPI-DING reference glasses for in situ microanalysis: New reference values for element concentrations and isotope ratios. Geochem. Geophy. Geosy. **2006**, *7*, 1–44.
13. Rodushkin, I.; Axelsson, M. D.; Malinovsky, D.; Baxter, D. C. Analyte- and matrix-dependent elemental response variations in laser ablation inductively coupled plasma mass spectrometry, Part 1. The roles of plasma and ion sampling conditions. J. Anal. At. Spectrom. **2002**, *17*, 1223–1230.
14. Kuhn, H. R.; Guillong, M.; Günther, D. Size-related vaporisation and ionisation of laser-induced glass particles in the inductively coupled plasma. Anal. Bioanal. Chem. **2004**, *378*, 1069–1074.
15. Fryer, B. J.; Jackson, S. E.; Longerich, H. P. The design, operation and role of the laser-ablation microprobe coupled with an inductively coupled plasma-mass spectrometer (LAM-ICP-MS) in the earth sciences. Can. Mineral. **1995**, *33*, 303–312.
16. Chen, Z. X. Inter-element fractionation and correction in laser ablation inductively coupled plasma mass spectrometry. J. Anal. At. Spectrom. **1999**, *14*, 1823–1828.
17. Liu, H. C.; Borisov, O. V.; Mao, X. L.; Shuttleworth, S.; Russo, R. E. Pb/U Fractionation during Nd:YAG 213 nm and 266 nm laser ablation sampling with inductively coupled plasma mass spectrometry. Appl. Spectros. **2000**, *54*, 1435–1442.
18. Motelica-Heino, M.; Coustumer, P. L.; Donard, O. F. X. Micro- and macro-scale investigation of fractionation and matrix effects in LA-ICP-MS at 1064 nm and 266 nm on glassy materials. J. Anal. At. Spectrom. **2001**, *16*, 542–550.
19. Jeffries, T. E.; Pearce, N. J. G.; Perkins, W. T.; Raith, A. Chemical fractionation during infrared and ultraviolet laser ablation inductively coupled plasma mass spectrometry—implications for mineral microanalysis. Anal. Comm. **1996**, *33*, 35–39.
20. Outridge, P. M.; Doherty, W.; Gregoire, D. C. Ablative and transport fractionation of trace elements during laser sampling of glass and copper. Spectrochim. Acta B **1997**, *52*, 2093–2102.
21. Kroslakova, I.; Günther, D. Elemental fractionation in laser ablation-inductively coupled plasma-mass spectrometry: Evidence for mass load induced matrix effects in the ICP during ablation of a silicate glass. J. Anal. At. Spectrom. **2007**, *22*, 51–62.
22. Longerich, H. P.; Günther, D.; Jackson, S. E. Elemental fractionation in laser ablation inductively coupled plasma mass spectrometry. Fresen. J. Anal. Chem. **1996**, *355*, 538–542.
23. Longerich, H. P.; Jackson, S. E.; Günther, D. Inter-laboratory note. Laser ablation inductively coupled plasma mass spectrometric transient signal data acquisition and analyte concentration calculation. J. Anal. At. Spectrom. **1996**, *11*, 899–904.
24. Ludwig, K. R. *ISOPLOT 3.0: A Geochronological Toolkit for Microsoft Excel*. Berkeley Geochronology Centre Special Publication No. 4, Berkeley, CA, USA, **2003**, 1–71.
25. Jochum, K. P.; Stoll, B.; Herwig, K.; Willbold, M. Validation of LA-ICP-MS trace element analysis of geological glasses using a new solid-state 193 nm Nd:YAG laser and matrix-matched calibration. J. Anal. At. Spectrom. **2007**, *22*, 112–121.
26. Jochum, K. P.; Dingwell, D. B.; Rocholl, A.; Stoll, B.; Hofmann, A. W. Thirty one others. The preparation and preliminary characterisation of eight geological MPI-DING reference glasses for in-situ microanalysis. Geostand. Newsl. **2000**, *24*, 87–133.